Available online at www.sciencedirect.com
ScienceDirect
International Journal of Heat and Mass Transfer 51 (2008) 618–629
International Journal of HEAT and MASS TRANSFER
www.elsevier.com/locate/ijhmt

Heat and mass transfer in plate-fin sinusoidal passages with vapor-permeable wall materials

Li-Zhi Zhang *

Key Laboratory of Enhanced Heat Transfer and Energy Conservation of Education Ministry, School of Chemical and Energy Engineering, South China University of Technology, Guangzhou 510640, China

Received 27 December 2006; received in revised form 4 April 2007
Available online 26 July 2007

Abstract

Laminar forced flow and heat mass transfer in sinusoidal plate-fin small passages encountered in compact heat mass exchangers are investigated. The duct is similar to a traditional plate-fin heat exchanger, but vapor-permeable materials like polymer membranes, paper, and ceramics can be used as the duct materials so both sensible heat and moisture can be exchanged simultaneously. Heat conduction and mass diffusion in the fins and heat and moisture convection in the fluid are analyzed simultaneously as a conjugate problem. Their fully developed Nusselt and Sherwood numbers under various aspect ratios and fin conductance parameters are calculated. The results found that though fins extend the heat transfer area, they are less effective compared to a traditional compact heat exchanger with metal foils. Most unfortunately, fin efficiencies for moisture transfer are even much smaller than those for heat transfer due to the low fin mass conductance parameters. For such heat mass exchangers, the use of fins can be regarded mostly as supporting materials, rather than as mass intensification techniques.

Keywords: Plate-fin ducts; Sine duct; Heat transfer; Mass transfer; Compact heat mass exchanger

1. Introduction

In recent years, various techniques have been applied to realize energy savings in buildings [1–3]. Among these promising technologies, air-to-air compact heat mass exchangers have been commercialized to recover both heat and moisture from exhaust air from air-conditioned buildings. In emulating a traditional compact surface heat exchanger, most of these products use plate-fin configurations, due to the reason that they are simple, compact, and mechanically strong even with very thin materials. Besides, these heat mass exchangers are cheaper than conventional metal heat exchangers since precious metal foils are saved. Fig. 1(a) shows the photo of a core used in a commercial heat mass exchanger. The structure, as shown in Fig. 1(b), is just like a traditional plate-fin compact heat exchanger. However, to transfer both sensible heat and moisture, some non-metal materials, like polymers, paper, and ceramics, have been used in place of the metal foils [4,5]. By this arrangement, water vapor can be transferred through these materials from one air stream to the other. For these exchangers, heat and mass transfer properties in the plate-fin passages are the key parameters affecting performance.

Plate-fin ducts with traditional well-conductive metal walls have been studied by many authors. A comprehensive review of the theoretical and experimental studies on fully developed forced convection and heat transfer in ducts of various cross sections up to the 1970s had been conducted by Shah and London [6], and documented in several well-known references [6–8]. Supplementary to these pioneering works, studies on heat transfer and fluid flow in ducts of other cross sections have been continued [9–11]. The results have been regarded as the basic data for heat exchanger design for these years. It should be noted that real fins have

* Tel./fax: +86 20 87114268.
E-mail address: Lzzhang@scut.edu.cn

0017-9310/$ - see front matter © 2007 Elsevier Ltd. All rights reserved.
doi:10.1016/j.ijheatmasstransfer.2007.04.050

Nomenclature

a	half duct height (m)
A_c	cross-sectional area (m^2)
A_t	transfer area (m^2)
b	half duct width (m)
c_p	specific heat (kJ kg^{-1} K^{-1})
d_h	hydraulic diameter (m)
D_{va}	vapor diffusivity in air (m^2/s)
D_{wf}	water diffusivity in fin material (m^2/s)
f	friction coefficient
h	convective heat transfer coefficient (kW m^{-2} K^{-1})
j	Chilton-Colburn j factor
k	mass transfer coefficient (m/s)
k_p	partition coefficient
L	length (m)
Le	Lewis number
M	total moisture transfer (kg/s)
n	number of channels for a flow
Nu	Nusselt number
Nu_T	Nusselt number for thermally fully developed laminar flow with T condition
P	pressure (Pa)
P_f	perimeter of duct (m)
Pr	Prandtl number
q	heat flux (kW m^{-2})
Q	total heat transfer (kW)
Re	Reynolds number
RH	relative humidity
Sc	Schmidt number
Sh	Sherwood number
Sh_ω	fully developed Sherwood number under uniform concentration condition
St	Stanton number
T	temperature (K)
u	velocity (ms^{-1})
U	velocity coefficient
V	volumetric flow rate (m^3/s)
W	water uptake (kg moisture/kg material)
x, y	dimensional transversal coordinates (m)
z	axial coordinate (m)

Greek symbols

δ	fin thickness (m)
ρ	density (kg m^{-3})
θ	dimensionless temperature
μ	dynamic viscosity (kg m^{-1} s^{-1})
Ω	conductance parameter
ψ	correction factor of temperature or humidity difference for cross flow
λ	heat conductivity (kW m^{-1} K^{-1})
η_{fin}	fin efficiency
ξ	dimensionless humidity
ω	humidity ratio (kg vapor/kg dry air)

Superscript

*	dimensionless

Subscripts

a	air
b	bulk
e	exhaust air
f	fin, fresh air
i	inlet
L	local, lower surface, moisture (latent heat)
m	mean
s	sensible heat
tot	total
u	upper surface
w	wall

limited conductance, which may comprise fin efficiencies. The effects of finite fin conductance on heat transfer have been investigated by several authors. Baliga and Azrak [12] carried out a numerical investigation of the forced convection and heat transfer in a triangular plate-fin duct. Heat conduction in the fin and forced convection in the fluid for both hydrodynamically and thermally fully developed flow were solved as a conjugate problem. The fin conductance parameters varied from 1.0 to infinitely large. To extend the studies to non-metal materials which have lower fin heat conductance parameters, in a recent work, the current author [13] investigated the developing and fully developed Nusselt numbers in a plate-fin triangular duct for fin conductance parameters from 0 to infinitely large, while considering thermal entry problems. Problems of the effects of finite fin conductance on heat transfer in other cross-sectional plate-fin ducts have not been addressed yet.

Besides heat transfer coefficients, to properly evaluate the heat mass exchanger performance, mass transfer coefficients are equally important. However, there has been no mention in this respect in literature up until now. Traditionally, mass transfer coefficients in a common pipe are obtained from heat transfer coefficients by heat mass transfer analogies, of which the most frequently cited one is the Chilton-Colburn Analogy [14]. According to this methodology, following equations can be used to estimate convective mass transfer coefficients in a pipe:

$$j_s = j_L \tag{1}$$

The Chilton-Colburn j factor for heat transfer [14]

$$j_s = St_s Pr^{2/3} \tag{2}$$

where Pr is the Prandtl number of air. Stanton number for heat transfer

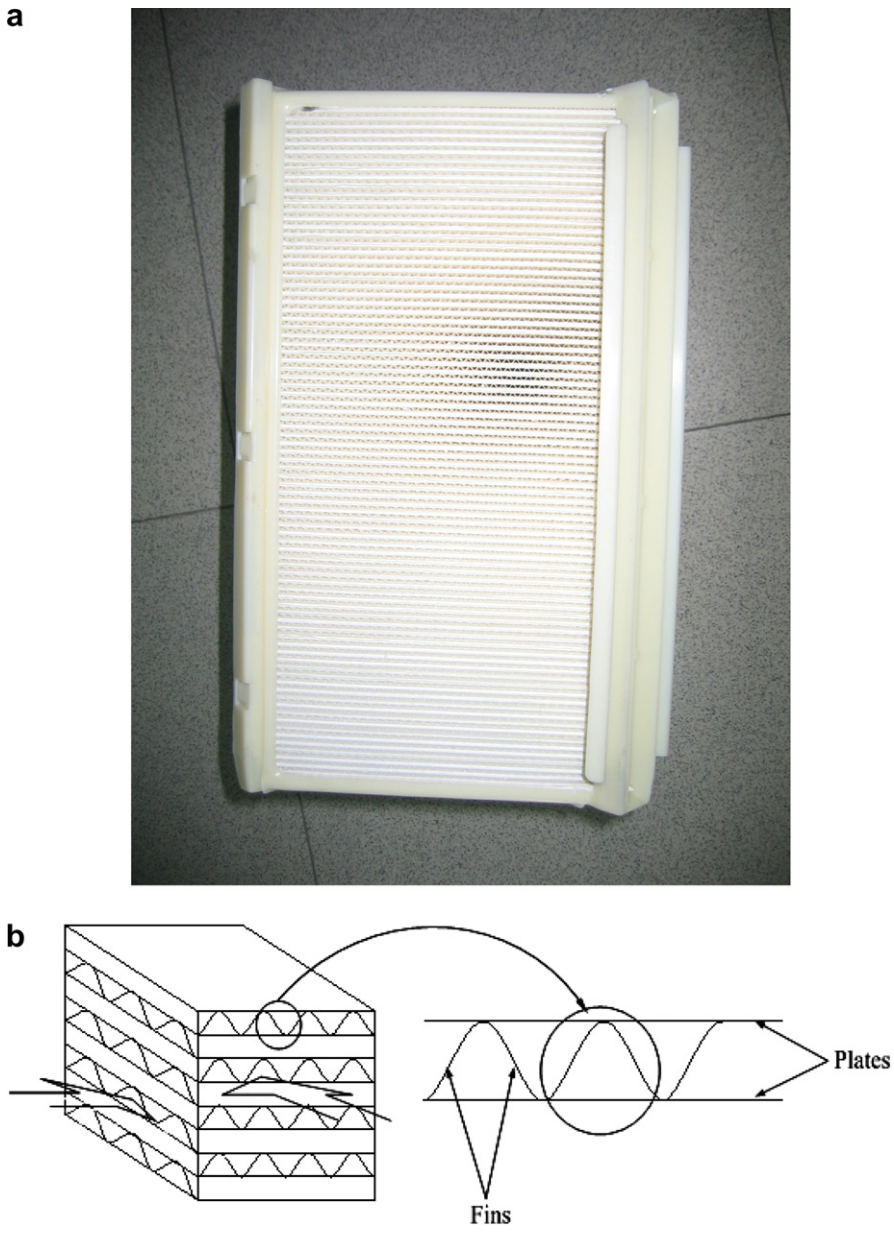

Fig. 1. Photo and schematic view of the core of a commercial plate-fin heat mass exchanger. (a) Photo of the core; (b) schematic of the duct.

$$St_s = \frac{h}{\rho_a c_p u} \tag{3}$$

where h is convective heat transfer coefficients (kW m^{-2} K^{-1}), u is air stream bulk velocity (m/s), c_p is specific heat (kJ kg^{-1} K^{-1}), ρ_a is dry air density (kg m^{-3}).

The convective heat transfer coefficient is also represented by a Nusselt number

$$Nu = \frac{hd_h}{\lambda} \tag{4}$$

where d_h is the hydrodynamic diameter of the channel (m), λ is thermal conductivity (kW m^{-1} K^{-1}).

The Chilton-Colburn j factor for mass transfer

$$j_L = St_L Sc^{2/3} \tag{5}$$

where Sc is the Schmidt number of moisture air. Stanton number for mass transfer

$$St_L = \frac{k}{\rho_a u} \tag{6}$$

where k is convective mass transfer coefficient (m/s).

Mass transfer in boundary layers is also described by a Sherwood number

$$Sh = \frac{kd_h}{D_{va}} \tag{7}$$

where D_{va} is vapor diffusivity in air (m^2/s). Substituting Eq. (2)–(7) into (1), a relation can be obtained

$$Sh = Nu \cdot Le^{-1/3} \tag{8}$$

$$Le = \frac{Pr}{Sc} \tag{9}$$

where Le is commonly called the Lewis number. For ventilation air and vapor mixture, which is always near atmospheric states, the Lewis number varies in the range of 1.19–1.22 [15], therefore it is usually approximate that $Sh = Nu$.

If above analogy still holds in our case, then the estimation of convective mass transfer coefficients would be simple. However, in plate-fin ducts used for non-metal heat mass exchanger, the fin conductance parameters for heat and mass transfer are so different that it is questionable that such an analogy still exists. It is therefore imperative to obtain the convective mass transfer coefficients and find the relations between the heat and mass transfer in such plate-fin ducts. This will be the objective of this research.

2. Governing equations

2.1. Momentum transfer

Sinusoidal duct is one of the most frequently used duct cross sections for plate-fin exchanger design. Fig. 2 shows the representing geometries for a duct: duct height $2a$; width $2b$; duct length, L; aspect ratio a/b. The duct is comprised of lower plate AC, and two sinusoidal fins AD and DC. The coordinate system for the two fins is s and y_1, which is tangential and normal to the fins, respectively. Their directions change from point to pint along the curved fins. Fin curve can be expressed as a sinusoidal function

$$y = a\left[1 - \cos\left(\frac{\pi}{b}x\right)\right] \tag{10}$$

The flow in the duct is considered to be laminar and hydrodynamically fully developed, but thermally and mass developing in the entrance region of the duct. The fluid is Newtonian with constant physical properties. Additionally, uniform plate temperature and uniform plate concentration boundary conditions are considered.

For fully developed laminar flow in ducts, the Navier–Stokes equations reduce to [14]

$$\mu\left(\frac{\partial^2 u}{\partial x^2} + \frac{\partial^2 u}{\partial y^2}\right) = \frac{\mathrm{d}P}{\mathrm{d}z} \tag{11}$$

where μ is dynamic viscosity (Pa s), P is the pressure (Pa), z is the axial coordinate (m).

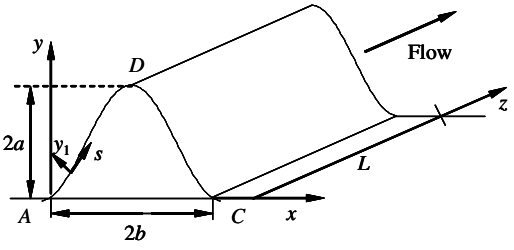

Fig. 2. Geometries of a plate-fin sinusoidal duct.

The above equation can be normalized to

$$\frac{\partial^2 u^*}{\partial x^{*2}} + \left(\frac{b}{a}\right)^2 \frac{\partial^2 u^*}{\partial y^{*2}} + \frac{4b^2}{d_\mathrm{h}^2} = 0 \tag{12}$$

with a dimensionless velocity

$$u^* = -\frac{\mu u}{(\mathrm{d}P/\mathrm{d}z)d_\mathrm{h}^2} \tag{13}$$

where hydraulic diameter

$$d_\mathrm{h} = \frac{4A_\mathrm{c}}{P_\mathrm{f}} \tag{14}$$

where A_c is the cross-section area of the duct (m^2), P_f is the perimeter of the duct (m).

Dimensionless coordinates are defined by

$$x^* = \frac{x}{2b} \tag{15}$$

$$y^* = \frac{y}{2a} \tag{16}$$

The characteristics of fluid flow in the duct can be represented by the product of the friction coefficient and the Reynolds number as

$$(fRe) = \left(-\frac{d_\mathrm{h}\frac{\mathrm{d}P}{\mathrm{d}z}}{2\rho u_\mathrm{m}^2}\right)\left(\frac{\rho u_\mathrm{m} d_\mathrm{h}}{\mu}\right) = \frac{1}{2u_\mathrm{m}^*} \tag{17}$$

where u_m^* is the average dimensionless velocity on a cross section, and it is calculated by

$$u_\mathrm{m}^* = \frac{\int\int u^* \mathrm{d}A}{A_\mathrm{c}} \tag{18}$$

2.2. Heat transfer

2.2.1. Air stream

Energy conservation in the fluid can be expressed by [14]

$$\rho_\mathrm{a} c_p u \frac{\partial T}{\partial z} = \lambda\left(\frac{\partial^2 T}{\partial x^2} + \frac{\partial^2 T}{\partial y^2}\right) \tag{19}$$

where T is fluid temperature (K).

The above equation can be normalized to

$$U\frac{\partial \theta}{\partial z^*} = \frac{\partial^2 \theta}{\partial x^{*2}} + \left(\frac{b}{a}\right)^2 \frac{\partial^2 \theta}{\partial y^{*2}} \tag{20}$$

with a dimensionless temperature

$$\theta = \frac{T - T_\mathrm{w}}{T_\mathrm{i} - T_\mathrm{w}} \tag{21}$$

where in the equations, T_i is the inlet temperature of the fluid, and T_w is the wall temperature. Dimensionless axial position is defined by

$$z^* = \frac{z}{d_\mathrm{h} Re\, Pr} \tag{22}$$

Velocity coefficient U is defined by

$$U = \frac{u^*}{u_\mathrm{m}^*}\frac{4b^2}{d_\mathrm{h}^2} \tag{23}$$

Dimensionless bulk temperature

$$\theta_b = \frac{\int\int u^* \theta \, dA}{\int\int u^* dA} \tag{24}$$

An energy balance in a control volume in the duct [14] will give the equation for estimation of the local Nusselt number as

$$Nu_L = -\frac{1}{4\theta_b}\frac{d\theta_b}{dz^*} \tag{25}$$

and the mean Nusselt number from $z^* = 0$ to z^* by

$$Nu_m = -\frac{1}{4z^*}\ln\theta_b \tag{26}$$

2.2.2. Fins

At any location along the fin, there is a balance between the net conduction along the fin and the heat transfer from the surface of the fin to the fluid. Heat transfer in fin is governed by the following one-dimensional model [12,13]:

$$\lambda_f \delta \frac{d^2 T_f}{ds^2} = q_u + q_L \tag{27}$$

$$q_u = -\lambda\left(\frac{\partial T}{\partial y_1}\right)_u \tag{28}$$

$$q_L = \lambda\left(\frac{\partial T}{\partial y_1}\right)_L \tag{29}$$

where λ_f is fin conductivity and λ is air conductivity, $(\partial T/\partial y_1)$ is the normal gradient of fluid temperature on the lower or upper surface of fin. The heat flux at the lower surface and the upper surface are skew symmetric [12,13], as schematically depicted in Fig. 3. The relation is mathematically expressed by

$$q_u|_s = -q_L|_{L_f - s} \tag{30}$$

where L_f is the length of a single curved fin AD.

Eqs. (27)–(30) can be combined and normalized to

$$\Omega_s \frac{d^2\theta_f}{ds^{*2}} = -\left(\frac{\partial\theta}{\partial y_1^*}\right)_{s^*} - \left(\frac{\partial\theta}{\partial y_1^*}\right)_{L_f^* - s^*} \tag{31}$$

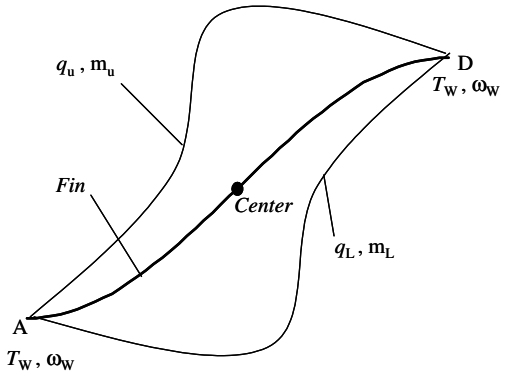

Fig. 3. Skew-symmetric heat and mass flux distributions on the upper and lower fin fluid interfaces.

where Ω_s is a dimensionless parameter named fin heat conductance parameter. It is defined by

$$\Omega_s = \frac{\lambda_f \delta}{\lambda(2a)} \tag{32}$$

where dimensionless fin temperature

$$\theta_f = \frac{T_f - T_w}{T_i - T_w} \tag{33}$$

and dimensionless coordinates

$$s^* = \frac{s}{2a} \tag{34}$$

$$y_1^* = \frac{y_1}{2a} \tag{35}$$

$$L_f^* = \frac{L_f}{2a} \tag{36}$$

2.3. Mass transfer

Air travels in the duct while exchanging moisture with duct walls. Mass conservation in the air stream can be expressed by

$$u\frac{\partial\omega}{\partial z} = D_{va}\left(\frac{\partial^2\omega}{\partial x^2} + \frac{\partial^2\omega}{\partial y^2}\right) \tag{37}$$

where ω is humidity ratio of air (kg vapor/kg dry air).

The above equation can be normalized to

$$U\frac{\partial\xi}{\partial z^*} = \frac{\partial^2\xi}{\partial x^{*2}} + \left(\frac{b}{a}\right)^2\frac{\partial^2\xi}{\partial y^{*2}} \tag{38}$$

where dimensionless humidity ratio

$$\xi = \frac{\omega - \omega_w}{\omega_i - \omega_w} \tag{39}$$

where in the equations, ω_i is the inlet air humidity, and ω_w is the humidity on wall surface.

Dimensionless bulk humidity

$$\xi_b = \frac{\int\int u^* \xi \, dA}{\int\int u^* dA} \tag{40}$$

Similarly, a mass balance in a control volume in the duct will give the equation for estimation of the local Sherwood number as

$$Sh_L = -\frac{1}{4\xi_b}\frac{d\xi_b}{dz^*} \tag{41}$$

and the mean Sherwood number from $z^* = 0$ to z^* by

$$Sh_m = -\frac{1}{4z^*}\ln\xi_b \tag{42}$$

Similar to heat conduction in the fin, at any location, there is a mass balance between the net water diffusion along the fin and the mass transfer from the surface of the fin to the fluid. The phenomenon is expressed by

$$D_{wf}\rho_f\delta\frac{d^2W}{ds^2} = m_u + m_L \tag{43}$$

$$m_u = -D_{va}\rho_a\left(\frac{\partial\omega}{\partial y_1}\right)_u \tag{44}$$

$$m_L = D_{va}\rho_a\left(\frac{\partial\omega}{\partial y_1}\right)_L \tag{45}$$

where D_{wf} is diffusivity of water in fin materials (m^2/s); ρ_f is density of fin materials (kg/m^3); W is water content in fin materials (kg water/kg dry material); m_u is moisture flux from upper surface of fin, and m_L is moisture flux from lower surface. $(\partial\omega/\partial y_1)$ is the normal gradient of vapor concentration on the lower or upper surface of fin. Due to symmetry, the mass flux at the lower surface and the upper surface are also skew symmetric. The relation is mathematically expressed by

$$m_u|_s = -m_L|_{L_f-s} \tag{46}$$

Water uptake in a hygroscopic material is a function of air relative humidity. Fig. 4 shows the measured sorption isotherm of the material used for the investigated heat mass exchanger [16]. The discrete dots are the measured data with a thermo-hygrostat. A polynomial curve can be regressed to represent this isotherm from 0% to 100% RH. The relation between RH and humidity ratio is

$$RH = 10^{-6}e^{5294/T}\omega \tag{47}$$

The temperature differences between two surfaces of a fin are quite small due to the small fin thickness [16]. For air conditioning industry, heat mass exchanger always works between 40%RH and 80%RH. Considering these factors, the relative humidity can be a linear expression of humidity ratio, and the sorption isotherm for the material can also be approximated by a linear equation as

$$W = k_p\omega \tag{48}$$

where k_p is defined as the partition coefficient.

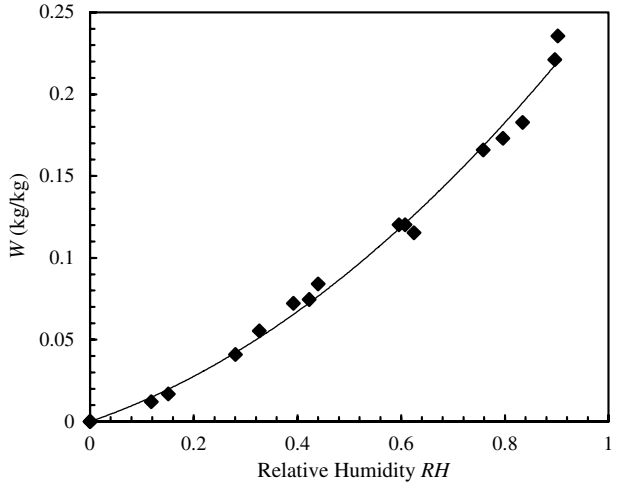

Fig. 4. Sorption isotherm for the core material in heat mass exchanger.

Substituting Eqs. (44)–(48) to (43) following dimensionless equation can be found:

$$\Omega_L\frac{d^2\xi_f}{ds^{*2}} = -\left(\frac{\partial\xi}{\partial y_1^*}\right)_{s^*} - \left(\frac{\partial\xi}{\partial y_1^*}\right)_{L_f^*-s^*} \tag{49}$$

where Ω_L is defined as the dimensionless fin mass conductance parameter. It is calculated by

$$\Omega_L = \frac{\delta\rho_f D_{wf}k_p}{\rho_a D_{va}(2a)} \tag{50}$$

where dimensionless humidity ratio in fins

$$\xi_f = \frac{\omega_f - \omega_w}{\omega_i - \omega_w} \tag{51}$$

It can be found that Eqs. (38) and (49) are in the same forms as Eqs. (20) and (31), respectively. Therefore, the solution of dimensionless humidity ratio can be an analogy to the solution of dimensionless temperature, if the fin mass conductance parameters are the same values as the fin heat conductance parameters. In other words, the solution of dimensionless humidity is the same as the dimensionless temperature, if assuming same values of heat and mass fin conductance parameters. Consequently, it is only necessary to solve either the heat transfer equations or the mass transfer equations.

2.4. Boundary conditions

The boundary conditions for fluid

$$u^* = 0, \quad \text{on all the walls of the duct} \tag{52}$$

$$\theta = 0 \quad \text{and} \quad \xi = 0, \quad \text{at } y^* = 0 \tag{53}$$

Inlet condition

$$\theta = 1 \quad \text{and} \quad \xi = 1, \quad \text{at } z^* = 0 \tag{54}$$

The boundary conditions for fins

$$\theta_f = 0 \quad \text{and} \quad \xi_f = 0 \quad \text{at } s^* = 0,\ L_f^* \tag{55}$$

Fin–fluid coupling:

$$\theta_f = \theta \quad \text{and} \quad \xi_f = \xi \text{ at fin–fluid interfaces} \tag{56}$$

3. Numerical solution

3.1. Solution procedure

The duct geometry is a sinusoidal one. For such non-rectangular shapes, a boundary-fitted coordinate transformation technique is used to transfer the irregular physical domain to a square computational domain. The basic idea of the boundary-fitted coordinate system is to have a coordinate system such that the body contour coincides with the coordinate lines. The transformation between the physical coordinates and the boundary-fitted coordinates, which is usually a square domain, is achieved by solving two Poisson equations on physical domain. For a detailed

introduction of a boundary-fitted coordinate system, please see Refs. [17,18].

The resulting grid constructions for the duct are shown in Fig. 5. To account for the drastic variations of temperature and mass concentration at duct inlet, grids are dense near inlet, while sparsely populated after thermal entry length.

When these mesh generations are completed, the governing differential equations (12), (20) and (31) were transformed from the original physical domain to the generated boundary fitted coordinate system. Then they were reduced to a set of algebraic equation systems, which can be solved by ADI techniques [13,19]. It is clear that iteration is needed to obtain the solution. In each direction, a tri-diagonal matrix is solved, by treating the non-linear cross-derivative, as a source term and using its values of last iteration. Although momentum equation in the finite difference form is solved only in two directions for the determination of the velocity distribution, the energy and mass equations must be solved at every step change in the flow direction to determine the temperature and concentration distribution. The proposed finite difference schemes are implicit numerical schemes.

After the solution of fluid velocity, temperatures in fluid and on two fins are solved on the generated grids, taking the current fluid temperature as the default boundary conditions. The whole calculating procedure can be summarized as the following:

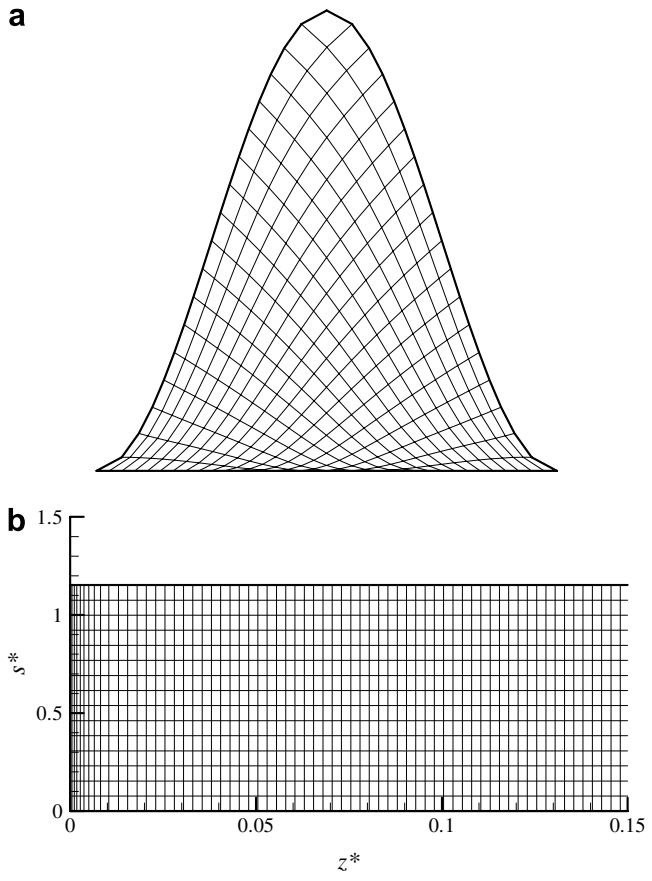

Fig. 5. Grid configurations for the duct. (a) Cross section, (b) duct length.

(a) Grid generation for both the fluid and the fins.
(b) Solve momentum equation (12). Get the velocity fields and resistance data for the duct.
(c) Assume initial temperature fields in the fluid.
(d) Taking current fluid temperature as the boundary conditions for fins. Get the temperature fields on two fins, by the solution of Eq. (31).
(e) Taking the current values of temperature on fins as the default values, get the temperature profiles in the fluid by solving Eq. (20).
(f) Go to (d), until the old values and the newly calculated values of temperature at all calculating nodes are converged.

As seen, the solution of velocity is only executed once before the calculation of temperature. After these procedures, all the governing equations are satisfied simultaneously. Then the local and mean Nusselt numbers are calculated. For mass transfer properties, if assuming Ω_L is the same value as Ω_s, Sh_L will equal to Nu_L. Correspondingly, the fully developed Sherwood number under uniform concentration boundary conditions Sh_ω is equal to Nu_T.

4. Results and discussion

4.1. Numerical validation

To assure the accuracy of the results presented, a grid independence test was performed for the duct to determine the effects of the grid size. It indicates that 21×21 grids on duct cross section and $\Delta z^* = 0.001$ axially are adequate (less than 0.1% difference compared with 31×31 grids and $\Delta z^* = 0.0005$).

To further validate the numerical program, ordinary ducts of various cross sections are calculated under uniform temperature conditions for all walls. Namely, ducts with ideal well-conductive fins are considered first. For hydrodynamically fully developed laminar flow in ducts, (fRe) is a constant. The local Nusselt numbers in the duct will decrease along the flow and reach stable values when the flow is thermally fully developed. The fully developed Nu values under uniform temperature conditions are denoted as Nu_T. The calculated values of (fRe) and Nu_T for these ordinary ducts are listed in Table 1. Comparisons are made with the values form well-known references [6–11]. As seen, the current study predicts the flow and heat transfer well. They are in accordance with the published data. Maximum uncertainty is less than 5%.

4.2. Flow and temperature fields

After the program is validated, sinusoidal ducts with one plate of uniform temperature and two fins coupling with fluid, as shown in Fig. 2, are modeled. Velocity and temperature fields in the fluid are obtained. Fig. 6 shows the velocity profile distribution on the duct cross section for $a/b = 0.5$. The values in the figure are dimensionless

Table 1
Fully developed (fRe) and Nusselt numbers for common ducts of various cross sections

Cross sections			(fRe)			Nu_T		
			Refs. [3–5]	This study	Error (%)	Refs. [3–5]	This study	Error (%)
Circular			16.0	15.86	0.8	3.657	3.68	0.6
Rectangular	a/b	0.125	20.5	20.32	0.9	5.60	5.73	2.3
		0.25	18.25	18.14	0.6	4.44	4.55	2.5
		0.5	15.50	15.30	1.3	3.39	3.45	1.8
		1.0	14.227	14.01	1.5	2.976	3.06	2.8
Isosceles triangular	a/b	0.289	13.243	12.87	2.8	2.301	2.262	1.7
		0.5	13.301	12.91	2.9	2.359	2.451	3.9
		0.866	13.321	13.39	0.5	2.500	2.596	3.7
		1.866	13.09	12.96	1.0	2.284	2.391	4.7
Sine	a/b	0.5	11.207	11.170	0.4	2.12	2.181	2.8
		0.75	12.234	12.213	0.2	2.33	2.372	1.7
		1.0	13.003	12.964	0.3	2.45	2.521	2.9
		1.5	14.002	14.115	0.8	2.6	2.573	1.1
		2.0	14.553	14.648	0.7	–	2.888	–

velocity u^*. As seen, in the center, the contours are near-circular, but in places near the boundaries, they are near-triangles. In the corners, there are dead spaces with little fluid flowing which will affect heat transfer finally. The flow shows a same pattern as that of a common sinusoidal duct.

The dimensionless temperature profiles in the fluid are shown in Figs. 7 and 8 for $\Omega_s = 0.5$ and 0.1, respectively. As seen, at higher fin heat conductance parameters, the temperature contours are more similar to those in ducts with three walls of uniform temperature. At lower fin conductance parameters, temperature contours show in majority a pattern of straight lines parallel to the plate, which is similar to temperature profiles in parallel-plates ducts. Besides, in the center, isotherms are in elliptical shapes. When Ω_s increases, the contours transform from parallel horizontal lines to circles, implicating increased heat transfer from fins to fluid.

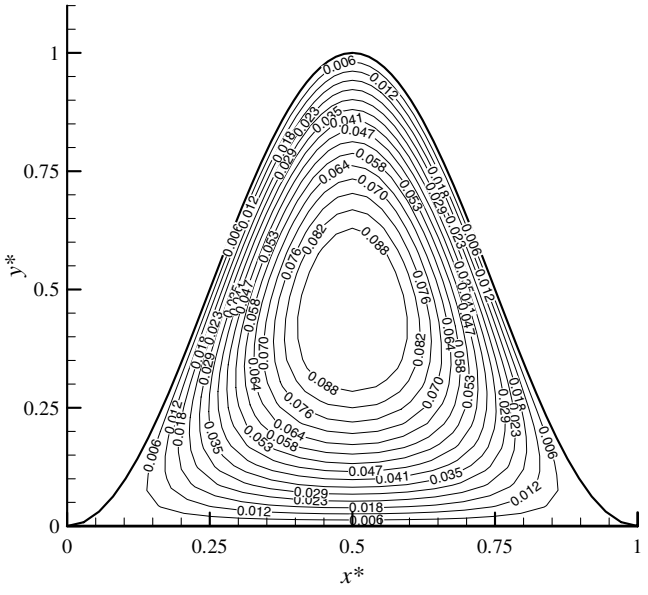

Fig. 6. Dimensionless velocity profiles (u^*) on duct cross section, $a/b = 0.5$.

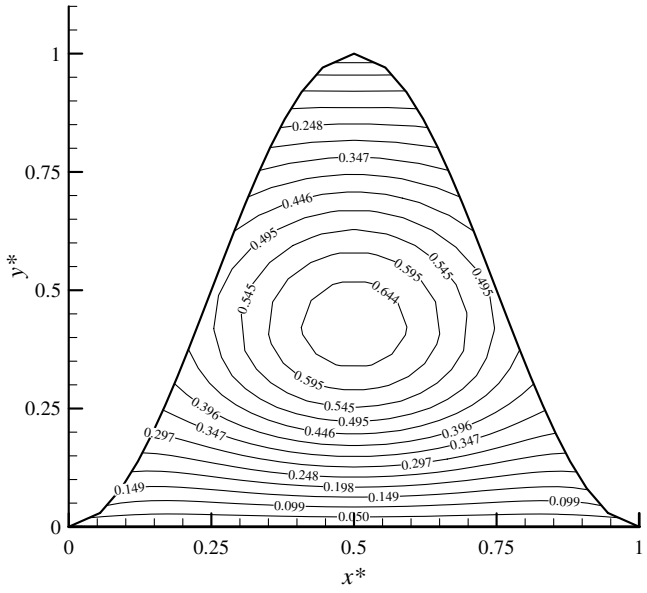

Fig. 7. Dimensionless temperature contours on duct cross section at $z^* = 0.1$ for $a/b = 0.5$ and $\Omega_s = 0.5$.

Dimensionless temperature profiles on the fins are shown in Figs. 9 and 10 for $\Omega_s = 0.5$ and 0.1, respectively. Temperatures at locations where fins connect with plate are equal to the plate temperature. Temperatures at other locations vary with fin heat conductance parameters. The higher the fin heat conductance parameters, the more homogeneous the temperature distributions on fins are. The lower the fin heat conductance parameters, the less heat transferred from fins to fluid. The isotherms on fins show a skew symmetric behavior as expected.

4.3. Nusselt and Sherwood numbers

Once the temperature fields in fluid has been determined, the dimensionless bulk temperature, the local Nusselt numbers, and the mean Nusselt numbers can be

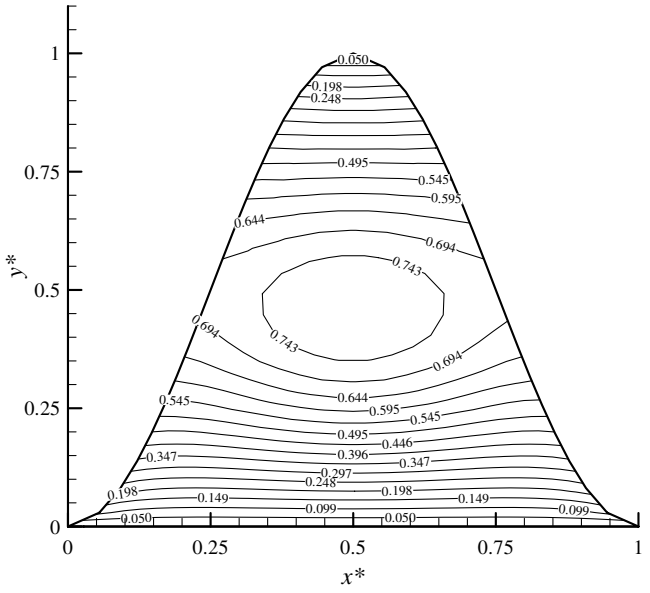

Fig. 8. Dimensionless temperature contours on duct cross section at $z^* = 0.1$ for $a/b = 0.5$ and $\Omega_s = 0.1$.

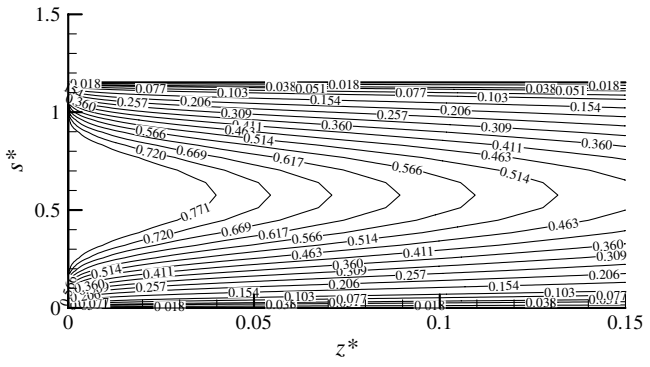

Fig. 9. Dimensionless temperature contours on fins for ducts of $a/b = 0.5$ and $\Omega_s = 0.5$.

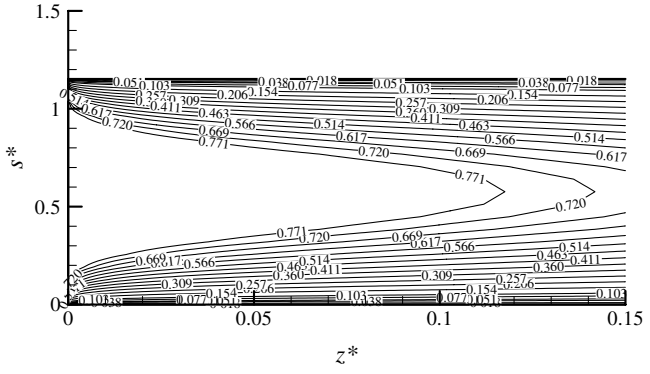

Fig. 10. Dimensionless temperature contours on fins for ducts of $a/b = 0.5$ and $\Omega_s = 0.1$.

calculated. Fig. 11 shows the axial variations of local Nusselt numbers with different fin heat conductance parameters. The axial position z^* is a dimensionless parameter

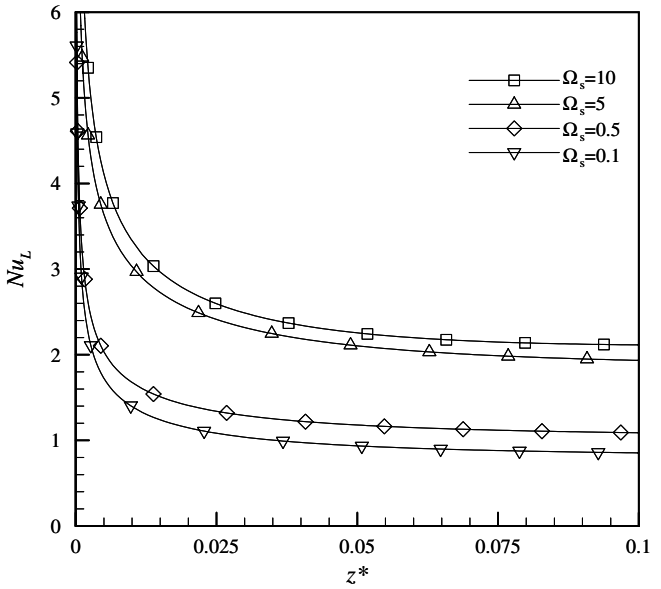

Fig. 11. Variations of Nu_L along flow axis for $a/b = 0.5$ with different fin heat conductance parameters.

reflecting duct length, diameter, Reynolds numbers and Prandtl numbers, as defined by Eq. (22). The local Nusselt number decreases from a high value at inlet, then it comes to a stable value Nu_T. This fully developed value varies with apex angles and fin conductance parameters. The higher the fin heat conductance parameters, the higher the Nu_T. After z^* is greater than 0.05, the flow can be considered fully developed.

Fin efficiency for heat transfer is defined as the ratio of Nu_T at a finite fin heat conductance to that at $\Omega_s = \infty$, or

$$\eta_{\text{fin}} = \frac{Nu_{T,\Omega_s}}{Nu_{T,\Omega_s=\infty}} \tag{57}$$

Fin efficiency for mass transfer is defined as the ratio of Sh_ω at a finite fin mass conductance to that at $\Omega_L = \infty$, or

$$\eta_{\text{fin}} = \frac{Sh_{\omega,\Omega_L}}{Sh_{\omega,\Omega_L=\infty}} \tag{58}$$

As the mass transfer equations are in the same forms as the heat transfer equations, fin efficiency for mass transfer will equal to that for heat transfer, if the fin mass conductance parameter is equal to the fin heat conductance parameter.

Table 2 lists the calculated Nu_T and/or Sh_ω and fin efficiencies for various aspect ratios and fin conductance parameters. They are the basic data that can be used for compact heat exchanger or heat mass exchanger design.

4.4. Experimental analysis

It is difficult to directly measure the local Nusselt numbers in the small channels. Instead, the inlet and outlet temperatures and humidities to and from the exchanger can be easily monitored. At this step, the mean Nusselt numbers

Table 2
Fully developed Nusselt/Sherwood numbers and fin efficiencies for plate-fin sinusoidal ducts of various aspect ratios

a/b	Ω_s / Ω_L	Nu_T / Sh_ω	η_{fin}	a/b	Ω_s / Ω_L	Nu_T / Sh_ω	η_{fin}
0.2	∞	1.551	1.0	0.5	∞	2.181	1.0
	25	1.523	0.982		25	2.133	0.978
	10	1.201	0.774		10	2.107	0.966
	5	1.033	0.666		5	1.908	0.875
	2	0.863	0.556		2	1.524	0.699
	1	0.791	0.510		1	1.260	0.578
	0.5	0.739	0.476		0.5	1.055	0.484
	0.1	0.694	0.447		0.1	0.824	0.378
	0	0.641	0.413		0	0.737	0.338
1.0	∞	2.521	1.0	2.0	∞	2.888	1.0
	25	2.492	0.988		25	2.714	0.940
	10	2.369	0.940		10	2.651	0.918
	5	2.167	0.860		5	1.922	0.666
	2	1.721	0.683		2	1.511	0.523
	1	1.379	0.547		1	1.194	0.413
	0.5	1.081	0.429		0.5	0.926	0.321
	0.1	0.751	0.298		0.1	0.631	0.218
	0	0.576	0.228		0	0.358	0.124
5.0	∞	2.586	1.0	5.0	1	1.015	0.392
	25	2.390	0.924		0.5	0.833	0.322
	10	2.170	0.839		0.1	0.661	0.256
	5	1.654	0.640		0	0.173	0.067
	2	1.274	0.493				

for the whole heat mass exchanger can be estimated. A simple test rig incorporating the core shown in Fig. 1(a) is set up. The test rig is shown in Fig. 12. Two air streams, representing fresh air and exhaust air, respectively, flow through the channels in the core while exchanging heat and moisture. Before they flow into the exchanger, their temperatures and humidities are adjusted to the desired set points. The air flow rates are controlled by the blowers and monitored by two flow meters. Equal air flow rates for the two streams are kept and heat mass balances are checked. The uncertainties are: temperature ±0.1 °C; humidity ±1%; volumetric flow rate ±0.5%.

The heat exchanged

$$Q = \rho_a V c_p (T_{fi} - T_{fo}) = \rho_a V c_p (T_{eo} - T_{ei}) \tag{59}$$

where V is volumetric flow rate (m^3/s). The total heat transfer coefficient is calculated by

$$h_{tot} = \frac{Q}{A_t n \Delta T_{lg}} \tag{60}$$

where A_t is the transfer area of a single channel (m), n is the number of channels for each stream, ΔT_{lg} is the log mean temperature difference between two streams (K), it is calculated by

$$\Delta T_{lg} = \psi_s \frac{(T_{fi} - T_{eo}) - (T_{fo} - T_{ei})}{\ln \frac{(T_{fi} - T_{eo})}{(T_{fo} - T_{ei})}} \tag{61}$$

where ψ_s is a correction factor of temperature difference for cross flow. Its specific value, which in this case is around 0.7–0.8, can be found graphically from [7].

The total heat transfer resistance includes the convective heat transfer resistance on both sides and the membrane itself, namely

$$\frac{1}{h_{tot}} = \frac{2}{h} + \frac{\delta}{\lambda_f} \tag{62}$$

From above equation, the convective heat transfer coefficient on each side h can be calculated. Then the mean Nusselt number for a single channel can be obtained from Eq. (4). This is the experimentally obtained Nusselt number.

Similarly, moisture transferred

$$M = \rho_a V (\omega_{fi} - \omega_{fo}) = \rho_a V c_p (\omega_{eo} - \omega_{ei}) \tag{63}$$

$$k_{tot} = \frac{M}{A_t n \Delta \omega_{lg}} \tag{64}$$

where $\Delta\omega_{lg}$ is the log mean humidity difference between two streams (kg/kg), it is calculated by

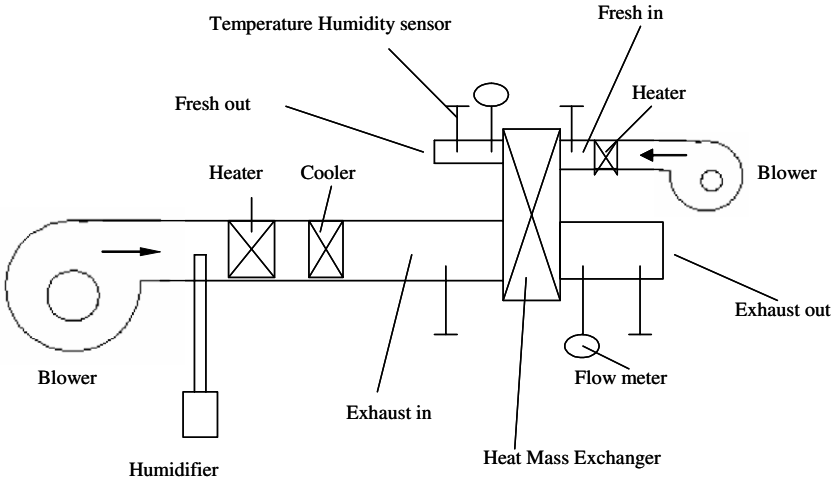

Fig. 12. Experimental set-up.

$$\Delta\omega_{lg} = \psi_L \frac{(\omega_{fi} - \omega_{eo}) - (\omega_{fo} - \omega_{ei})}{\ln \frac{(\omega_{fi} - \omega_{eo})}{(\omega_{fo} - \omega_{ei})}} \quad (65)$$

where ψ_L is a correction factor of mass difference for cross flow. The total moisture transfer resistance includes the convective mass transfer resistance on both sides and the membrane itself, namely

$$\frac{1}{k_{tot}} = \frac{2}{k} + \frac{\rho_a}{\rho_f} \cdot \frac{\delta}{D_{wf}} \quad (66)$$

From above equation, the convective mass transfer coefficient k can be calculated. Then the mean Sherwood number can be obtained from Eq. (7). This value is the experimentally obtained Sherwood number.

The geometries of the core tested are: duct height, 2 mm; aspect ratio 0.5; fin thickness, 0.1 mm; $n = 82$ (rows) $\times$ 74 (ducts per row); duct length, 15 cm. The operating conditions are: $V = 0.02$–$0.07\ m^3/s$; fresh air inlet set points, 35 °C, and 60%RH; exhaust air inlet set points, 25 °C, and 50%RH. The properties for material are measured in the laboratory in a separate study: $k_p = 10.6$; $D_{wf} = 4.5 \times 10^{-11}\ m^2/s$; $\lambda_f = 0.32\ W\ m^{-1}\ K^{-1}$; $\rho_f = 836\ kg/m^3$. With these parameters, the calculated fin heat conductance parameter Ω_s is 0.61, and the mass conductance parameter Ω_L is nearly 0 (exact value is 5.8×10^{-4}). The experimentally obtained Nusselt and Sherwood numbers for different flow rates are listed in Table 3 and compared with the numerically obtained mean values.

As seen, in the experiment, the z^* at the end of the duct is far larger than 0.05, therefore the flow is fully developed and the thermal entry influences are small. The mean Nusselt and Sherwood numbers are approximately equal to their fully developed values. The higher the air flow rates are, the longer the thermal entry length is, and the higher the mean Nusselt and Sherwood numbers are, because heat mass transfer coefficients are larger at inlets. The experiments underestimate the performance by around 10%, due to heat loses through surroundings and mass permeation through pinholes in the core, especially at low flow rates. Generally, the obtained experimental values are in accordance with the numerical values. This is another validation of the program.

4.5. Comparisons of heat and mass transfer

As defined by Eqs. (32) and (50), fin heat conductance parameters are determined by duct geometry and heat conductivity of fin materials. Table 4 lists the values of fin heat conductance parameters for some frequently encountered materials, including metal and non-metals, for a sinusoidal duct of height 2 mm, aspect ratio 0.5, and fin thickness 0.1 mm, as mentioned above. As seen, for almost all the metals, the fin heat conductance parameters are larger than 100, and the resulting fin heat efficiencies can be as high as 0.90–0.98. For such traditional metal compact heat exchangers, the influences of finite fin heat conductance on heat transfer are negligible. Direct utilization of heat transfer properties for a common duct is acceptable. For the recently commercialized compact heat mass exchangers which use non-metals to simultaneously transfer heat and moisture, the fin heat conductance parameters are usually less than 1.0, and the resulting fin efficiencies for heat transfer can be as low as 0.40. Though it is true that the fins still participate in the heat transfer enhancement, at least partially, at this stage, the effects of finite fin heat conductance on heat transfer will be substantial.

Similarly, as defined by Eq. (50), fin mass conductance parameters are determined by duct geometry and mass diffusivity of moisture in fin materials. Moisture diffusivity in air is around $2.5 \times 10^{-5}\ m^2/s$ [15]. Besides the test data in our experiment for the core material, a literature review found that moisture diffusivities in most non-metal hygroscopic materials are in or less than the order of $10^{-10}\ m^2/s$. For example, water diffusivities are from 0.5×10^{-12} to $1.5 \times 10^{-12}\ m^2/s$ in a PSS-Na/Al_2O_3 composite silicate [20]; from $8.0 \times 10^{-10}\ m^2/s$ to $5.0 \times 10^{-12}\ m^2/s$ in a Nafion polymer membrane [21]; and from $1.0 \times 10^{-13}\ m^2/s$ to

Table 4
Values of fin heat conductance parameter for some fin materials with duct height, 2 mm; aspect ratio 0.5, fin thickness, 0.1 mm; fluid, air

Fin materials	λ_f (W m^{-1} K^{-1})	Ω_s
Pure copper	401	751.00
Bronze	52	97.40
Iron	80.2	150.20
Steel	60.5	113.30
Aluminium	237	443.90
Carbon	1.6	3.00
Plywood	0.12	0.22
Wood	0.16	0.30
Clay	1.3	2.43
Glass	1.4	2.66
Paper	0.18	0.34
Teflon	0.35	0.66
Polymer membrane	0.13	0.24

Table 3
Comparisons of duct mean Nusselt and Sherwood numbers, experimentally and numerically obtained

V (m^3/s)	Re	z^*	Nu_m		Sh_m	
			Experimental	Numerical	Experimental	Numerical
0.023	102.3	1.28	1.01	1.13	0.703	0.738
0.034	151.8	0.86	1.13	1.20	0.721	0.741
0.046	205.7	0.64	1.18	1.23	0.756	0.767
0.052	232.1	0.56	1.23	1.27	0.771	0.794
0.061	272.8	0.48	1.25	1.32	0.811	0.832
0.068	303.6	0.43	1.29	1.34	0.842	0.863

1.0×10^{-12} m^2/s in a methylcellulose film [22]. The densities of these materials are in the order of 1000 kg/m^3. The partition coefficients are in the order of 10, or 15–20% water uptake under 60% RH. Based on these properties, the values of fin mass conductance parameters are in the order of 10^{-3}. With such low mass conductance parameters, the fin efficiencies for mass transfer will be below 0.1–0.2. Under such circumstances, nearly all the mass transfer between the two air streams will be accomplished by the plate, rather than by the fins. The fins seem to behave only like supporting materials, if excluding their role in partial participation in heat transfer. In engineering, sometimes supporting materials or spacers are necessary to separate the two streams because the plates are thin and soft.

In designing novel heat mass exchangers, it is simple to emulate a common compact heat exchanger with such a plate-fin configuration. However, the effectiveness of fins on heat transfer will be strongly compromised. Even worse, it has little use in enhancing mass transfer. Consequently, novel configurations such as the so-called cross-corrugated triangular ducts may provide a promising choice [23,24], since in this concept the two fluids directly exchange heat and moisture through all the three walls, in addition to intensification by flow turbulence.

5. Conclusions

For almost all the metal materials, the fin efficiencies for heat transfer can be as high as 0.90–0.98. The influences of finite fin heat conductance on heat transfer are negligible. However, for non-metal materials used in the novel heat mass exchanger, the fin efficiencies for heat transfer can be as low as 0.40. At this stage, the effects of finite fin conductance on heat transfer will be substantial.

The mass transfer equations can be expressed in the same forms as the heat transfer equations in a plate-fin heat mass exchanger. However, due to the large differences in values of heat and mass conductance parameters, a simple heat mass analogy which is apt to a common pipe fails to predict the mass transfer performance. Sherwood numbers in the plate-fin ducts are much smaller than the Nusselt numbers. This implicates that though it is simple in emulating a traditional compact heat exchanger, this structure is not an ideal configuration for heat mass exchanger, especially from the perspective of mass transfer.

Acknowledgements

The Project is supported by National Natural Science Foundation of China (50676034), and Fok Ying Tung Education Foundation (101057).

References

[1] Y.P. Zhang, G.B. Zhou, K.P. Lin, Q.L. Zhang, H.F. Di, Application of latent heat thermal energy storage in buildings: state-of-the-art and outlook, Build. Environ. 42 (2007) 2197–2209.

[2] Y.P. Zhang, X. Xu, H.F. Di, K.P. Lin, Experimental study on the thermal performance of the shape-stabilized phase change material floor used in passive solar buildings, ASME J. Solar Energy Eng. 128 (2006) 255–257.

[3] B.J. Chen, X. Wang, Y.P. Zhang, H. Xu, R. Yang, Experimental research on laminar flow performance of phase change emulsion, Appl. Therm. Eng. 26 (2006) 1238–1245.

[4] K.R. Kistler, E.L. Cussler, Membrane modules for building ventilation, Chem. Eng. Res. Des. 80 (2002) 53–64.

[5] L.Z. Zhang, J.L. Niu, Effectiveness correlations for heat and moisture transfer processes in an enthalpy exchanger with membrane cores, ASME J. Heat Transfer 122 (5) (2002) 922–929.

[6] R.K. Shah, A.L. London, in: Laminar Flow Forced Convection in Ducts, Academic Press Inc., New York, 1978, pp. 253–260.

[7] F.P. Incropera, D.P. Dewitt, in: Introduction to Heat Transfer, third ed., John Wiley & Sons, New York, 1996, p. 416 (Chapter 8).

[8] R.K. Shah, M.S. Bhatti, Laminar Convection Heat Transfer In Ducts, in: S. Kakac, R.K. Shah, W. Aung (Eds.), Handbook of Single-Phase Convective Heat Transfer, Wiley, New York, 1987.

[9] C.W. Leung, S.D. Probert, Forced convective turbulent flows through horizontal ducts with isosceles triangular internal cross sections, Appl. Energy 57 (1997) 13–24.

[10] S. Chen, T.L. Chan, C.W. Leung, Numerical prediction of laminar forced convection in triangular ducts with unstructured triangular grid method, Numer. Heat Transfer, Part A 38 (2000) 209–224.

[11] S.W. Ahn, K.P. Son, Heat transfer and pressure drop in the roughened equilateral triangular duct, Int. Commun. Heat Mass Transfer 29 (2002) 479–488.

[12] B.R. Baliga, R.R. Azrak, Laminar fully developed flow and heat transfer in triangular plate-fin ducts, ASME J. Heat Transfer 108 (1986) 24–32.

[13] L.Z. Zhang, Laminar flow and heat transfer in plate-fin triangular ducts in thermally developing entry region, Int. J. Heat Mass Transfer 50 (7–8) (2007) 1637–1640.

[14] R. Taylor, R. Krishna, in: Multicomponent Mass Transfer, John Wiley & Sons Inc., New York, 1993.

[15] W.M. Kays, M.E. Crawford, in: Convective Heat and Mass Transfer, third ed., McGraw-Hill Inc., New York, 1990.

[16] L.Z. Zhang, Y. Jiang, Y.P. Zhang, Membrane-based humidity pump: performance and limitations, J. Membr. Sci. 171 (2000) 207–216.

[17] J.F. Thompson, F. Thames, C. Martin, Automatic numerical generation of body-filled curvilinear coordinate system for field containing any number of arbitrary two-dimensional bodies, J. Comput. Phys. 24 (1974) 299–319.

[18] P.D. Thomas, J.F. Middlecoff, Direct control of grid point distribution in meshes generated by elliptic equations, AIAA J. 18 (1982) 652–656.

[19] J.L. Niu, L.Z. Zhang, Heat transfer and friction coefficients in corrugated ducts confined by sinusoidal and arc curves, Int. J. Heat Mass Transfer 45 (2002) 571–578.

[20] P. Aranda, W.J. Chen, C.R. Martin, Water transport across polystyrenesulfonate/alumina composite membranes, J. Membr. Sci. 99 (1995) 185–195.

[21] X.H. Ye, M.D. LeVan, Water transport properties of Nafion membranes. Part I: Single tube membrane module for air drying, J. Membr. Sci. 221 (2003) 147–161.

[22] F. Debeaufort, A. Voilley, P. Meares, Water vapor permeability and diffusivity through methylcellulose edible films, J. Membr. Sci. 91 (1994) 125–133.

[23] L.Z. Zhang, Convective mass transport in cross-corrugated membrane exchangers, J. Membr. Sci. 260 (2005) 75–83.

[24] L.Z. Zhang, Numerical study of periodically fully developed flow and heat transfer in cross-corrugated triangular channels in transitional flow regime, Numer. Heat Transfer, Part A: Appl. 48 (2005) 387–405.